An Analysis of Parton Distribution Functions of the Pion and the Kaon with the Maximum Entropy Input

Chengdong Han,^{1,2} Gang Xie,^{1,3} Rong Wang,^{1,2,*} and Xurong Chen^{1,2,3,†}

¹Institute of Modern Physics, Chinese Academy of Sciences, Lanzhou 730000, China
²School of Nuclear Science and Technology, University of Chinese Academy of Sciences, Beijing 100049, China
³Guangdong Provincial Key Laboratory of Nuclear Science, Institute of Quantum Matter,
South China Normal University, Guangzhou 510006, China
(Dated: May 27, 2022)

We present pion and kaon parton distribution functions from an global QCD analysis of the experimental data, using the DGLAP equations with parton-parton recombination corrections and the valence input of uniform distribution which maximizes the information entropy. At our input scale Q_0^2 , there are no sea quark and gluon distributions. All the sea quarks and gluons of the pion and the kaon are completely generated from the parton splitting precesses. The mass-dependent parton splitting kernel is applied for the strange quark distribution in the kaon. The obtained valence quark and sea quark distributions at high Q^2 ($Q^2 > 5$ GeV²) are compatible with the existed experimental measurements. Furthermore, the asymptotic behaviours of parton distribution functions at small and large x have been studied for both the pion and the kaon. Lastly, the first three moments of parton distributions at high Q^2 scale are calculated, which are consistent with other theoretical predictions.

I. INTRODUCTION

Pion and kaon, as the pseudo-Goldstone bosons [1, 2], are the important objects in understanding the dynamical chiral symmetry breaking. As the mass low-lying mesons, their internal structures are crucial for us to figure out the emergence of hadron mass from quantum chromodynamics (QCD) of strong interaction [3–6], in combination with the inquiring of the origin of proton mass [7–10]. Pion, as the lightest meson, plays a dominant role in mediating the nuclear force. Kaon, having a heavier strange quark inside, is interesting for us to see the interference between the emergence of mass from QCD and the Higgs mechanism [11]. The study on pion and kaon structures is an important way to test the nonperturbative QCD approaches, and to help answering the fundamental question on the origin of the hadron mass. Parton distribution functions (PDFs) are the conventional and useful way displaying the longitudinal momentum structure in the infinite momentum frame. In theory, there are actually quite a lot of methods giving the pion and kaon PDFs from different pictures, such as lattice QCD (LQCD) [12-15], Dyson-Schwinger Equations (DSE) [16–18], holographic QCD [19], light-front quantization [20], and constituent quark model [21–23].

In experiment, much less is known for the internal quark and gluon structures of the pion and the kaon, due to the absence of the fixed pion or kaon target. The current available data come from the pion or kaon beam induced Drell-Yan (DY) process on the nuclear target at CERN (NA3 and NA10) [24–26] and Fermilab (E615) [27], and the leading neutron deep inelastic scattering

process (LN-DIS) in e-p collision at HERA (ZEUS and H1) [28, 29]. Thanks to the HERA experimental measurement at small x, the sea quark and gluon distributions are much better constrained. But still, the fully kinematic overlap is preferred between the large x region accessed by DY process and the small x region accessed by LN-DIS process. For the kaon, the data is very scarce and they are from the NA3 DY measurement more than 40 years ago. More precise measurements from the DY process are still expected. The small x data of the pion and the kaon with a better kinematic coverage to the current DY data from the e-p process are also highly needed.

Although the data on pion and kaon structures are scarce, there are some pioneering works of the global QCD analyses of the pion PDFs. The previous analyses of GRS [30] and SMRS [31] constrain well the pion PDFs at $x \gtrsim 0.1$ using π -A scattering data with the dilepton (DY) and the prompt photon productions. Recently, the JAM collaboration [32] includes the DY data and the LN-DIS data in the analysis. By using a Bayesian Monte Carlo method, JAM collaboration finds that the uncertainties of sea quark and gluon distributions are huge with only DY data. With the inclusion of the leading neutron electroproduction data from HERA, the sea quark and gluon distributions are better constrained. The gluon distribution at small x is found to be much higher than the analysis inferred from DY data alone. The other significant finding is that the pion PDFs from the global analysis describe amazingly well the $\bar{d}-\bar{u}$ asymmetry in the proton [33], within the same pion cloud model of the chiral splitting function of $p \to n\pi^+$ [32]. The xFitter collaboration [34] finds that the current data are not enough to determine sea quark and gluon distributions unambiguously. Moreover, they explored the theoretical uncertainties from such as varying the renormalization and factorization scales, and from the flexibility of the chosen parametrization. The conclusion is

^{*} rwang@impcas.ac.cn

[†] xchen@impcas.ac.cn

that the valence distribution is well constrained, while the total uncertainty of experimental and theoretical uncertainties are large for the sea quark and gluon distributions. Last but not least, an interesting analysis of the DY data only finds that the power law of (1-x) at large $x \to 1$ limit agrees with the perturbative QCD prediction [35–37], when the soft-gluon resummation correction is considered [38].

In this work, to better fix the sea quark and gluon distributions, we try to perform a global analysis based on the dynamical parton model [39, 40]. In our dynamical parton model, the sea quark and gluon distributions are purely generated from the QCD evolution, which means that we assume there are no intrinsic sea quarks and gluons at the sufficiently low scale being the input scale Q_0^2 . In this way, the theoretical uncertainty from the flexibility of parametrization of initial sea quark and gluon distributions are removed. Starting from a very low scale around 0.1 GeV², we use the state-of-art processindependent renormalization-group-invariant strong coupling α_s in the analysis [41]. This type of strong coupling saturates at the infrared region of interaction. Due to the low resolution scale, the parton overlapping and the parton-parton recombination effect should not be ignored [40, 42–44]. Therefore, we use the parton-parton recombination corrected DGLAP equations in order to slow down the parton splitting processes. For the QCD evolution in terms of the strange quark, the mass-dependent DGLAP kernel [11, 45] is taken into account since the current strange quark mass is heavy, especially at the low scale. Regardless of the few experimental data of the kaon, the purely dynamical sea quark and gluon distributions of the kaon generated in standard QCD evolution in this work are the reliable predictions under the dynamical parton model. With the global analysis of the purely dynamical sea and gluons, we will get the better constrained sea quark and gluon distributions for both the pion and the kaon. We will present also the difference between strange valence distribution and up valence distribution in the kaon caused by the mass correction of the parton splitting kernel [11, 45]. Finally, we will also focus on the large-x and small-x behaviors of pion and kaon PDFs.

The organization of the paper is as follows. Section II introduces the nonperturbative input used in this global analysis based on the dynamical parton model. In Sec. III, we discuss the DGLAP equations with parton-parton recombination corrections and the saturating running strong coupling α_s , considering the effective mass of the gluon in the infrared region. Section IV shows the result of the global fit, the optimal hadronic scale Q_0^2 , and the optimal R for the magnitude of two parton recombination process. Section V illustrates the global fitting result compared with the experimental data, the resulting large-x and small-x behaviors of the PDFs of the pion and the kaon, and the predictions of the dynamical sea quark and gluon distributions. At the end, a short summary is given in Sec. VI.

II. NONPERTURBATIVE INPUT FROM MAXIMUM ENTROPY METHOD

In the global analysis of PDFs, the nonperturbative input is the parton distribution functions at the initial scale Q_0^2 . The PDFs at any higher Q^2 are calculated from the nonperturbative input with the QCD evolution equations which describe the Q^2 -dependence of PDFs. One of the main tasks in the global analysis is to find the optimal nonperturbative input which reproduces well the experimental data measured at the hard scale ($Q^2 \gtrsim 5$ GeV²). In the dynamical parton model, the input scale Q_0^2 is usually chosen to be closer to the hadronic scale $(\sim 0.1 \text{ GeV}^2)$, where only the valence quarks (constituent quarks) can be found in the hadron. There are two benefits of using the dynamical parton model. First, the nonperturbative input can be related to the simple quark model predictions. Second, the sea quark and gluon distributions are completely generated from the QCD evolution quations, which could be constrained much better with the few experimental data published so far.

At the hadronic scale, the pion plus has only one up quark and one anti-down quark. Therefore we have the following valence number sum rule and momentum sum rule for π^+ :

$$\int_{0}^{1} u_{V}^{\pi}(x, Q_{0}^{2}) dx = 1,$$

$$\int_{0}^{1} \bar{d}_{V}^{\pi}(x, Q_{0}^{2}) dx = 1,$$

$$\int_{0}^{1} x [u_{V}^{\pi}(x, Q_{0}^{2}) + \bar{d}_{V}^{\pi}(x, Q_{0}^{2})] dx = 1.$$
(1)

Similarly we have the following constraints for the non-perturbative input of K^+ at the hadronic scale:

$$\int_{0}^{1} u_{V}^{K}(x, Q_{0}^{2}) dx = 1,$$

$$\int_{0}^{1} \bar{s}_{V}^{K}(x, Q_{0}^{2}) dx = 1,$$

$$\int_{0}^{1} x [u_{V}^{K}(x, Q_{0}^{2}) + \bar{s}_{V}^{K}(x, Q_{0}^{2})] dx = 1.$$
(2)

The above nonperturbative inputs have the minimum number of components of the hadrons, however the functions of the initial parton distributions are still unknown. Using the maximum entropy method and taking the charge symmetry $u_{\rm V}^{\pi}(x,Q_0^2)=\bar{d}_{\rm V}^{\pi}(x,Q_0^2)$, the nonperturbative input is evaluated to be the uniform distribution [46, 47], which is written as,

$$u_{\rm V}^{\pi}(x, Q_0^2) = \bar{d}_{\rm V}^{\pi}(x, Q_0^2) = 1.$$
 (3)

In the maximum entropy approach, the information entropy of the initial quark distributions is taken to be at the maximum. Assuming SU(3) flavor symmetry, the nonperturbative input of the kaon is also the uniform

distribution from the maximum entropy method, which is written as,

$$u_{\mathcal{V}}^{\mathcal{K}}(x, Q_0^2) = \bar{s}_{\mathcal{V}}^{\mathcal{K}}(x, Q_0^2) = 1.$$
 (4)

With the initial quark distributions of the maximum entropy, the last thing for the nonperturbative input is to determine the input hadronic scale Q_0^2 . For the proton, the hadronic scale with only valence components is around $Q_0^2 = 0.07 \text{ GeV}^2$ [40], from a global analysis of the l-p DIS data. The hadrons of different sizes may have different initial resolution scales Q_0^2 . Therefore in this analysis of the PDFs of pseudoscalar mesons, the input hadronic scale is regarded as a free parameter which should be fixed from the global fit.

III. DGLAP EQUATIONS WITH PARTON-PARTON RECOMBINATION CORRECTIONS

To connect the nonperturbative input with the experimental measurements in the asymptotic region, the QCD evolution equations are needed. Usually, the Dokshitzer-Gribov-Lipatov-Altarelli-Parisi (DGLAP) equations [48– 50] are used to describe the Q^2 -dependence of PDFs. For the parton evolution starting from a very low Q_0^2 , the high twist corrections should not be neglected. The high twist effect can be modeled with the DGLAP equations with parton-parton recombination corrections. The parton-parton recombination effect was first put forward by Gribov, Levin and Ryskin (GLR) [42], then followed by Mueller, Qiu (MQ) evaluating the recombination coefficients with the covariant field theory [43]. Recently, the full recombination corrections (gluon-gluon, quark-gluon, quark-quark) were derived by Zhu, Ruan, and Shen using the time ordered field theory [51–53].

The DGLAP equations with parton-parton recombination corrections used in this work are given by [40, 44],

$$Q^2 \frac{dx f_{q_i}(x, Q^2)}{dQ^2} = \frac{\alpha_s(Q^2)}{2\pi} P_{qq} \otimes f_{q_i}, \tag{5}$$

for valence quark distributions,

$$Q^{2} \frac{dx f_{\bar{q}_{i}}(x, Q^{2})}{dQ^{2}} = \frac{\alpha_{s}(Q^{2})}{2\pi} [P_{qq} \otimes f_{\bar{q}_{i}} + P_{qg} \otimes f_{g}]$$

$$- \frac{\alpha_{s}^{2}(Q^{2})}{4\pi R^{2} Q^{2}} \int_{x}^{1/2} \frac{dy}{y} x P_{gg \to \bar{q}}(x, y) [y f_{g}(y, Q^{2})]^{2}$$

$$+ \frac{\alpha_{s}^{2}(Q^{2})}{4\pi R^{2} Q^{2}} \int_{x/2}^{x} \frac{dy}{y} x P_{gg \to \bar{q}}(x, y) [y f_{g}(y, Q^{2})]^{2},$$
(6)

for sea quark distributions, and

$$Q^{2} \frac{dx f_{g}(x, Q^{2})}{dQ^{2}} = \frac{\alpha_{s}(Q^{2})}{2\pi} [P_{gq} \otimes \Sigma + P_{gg} \otimes f_{g}]$$

$$-\frac{\alpha_{s}^{2}(Q^{2})}{4\pi R^{2} Q^{2}} \int_{x}^{1/2} \frac{dy}{y} x P_{gg \to g}(x, y) [y f_{g}(y, Q^{2})]^{2}$$

$$+\frac{\alpha_{s}^{2}(Q^{2})}{4\pi R^{2} Q^{2}} \int_{x/2}^{x} \frac{dy}{y} x P_{gg \to g}(x, y) [y f_{g}(y, Q^{2})]^{2},$$
(7)

for gluon distribution, where P_{qq} , P_{qg} , P_{gq} , P_{gg} are the standard parton splitting kernels, and $P_{gg \to \bar{q}}$, $P_{gg \to g}$ are the gluon-gluon recombination coefficients which can be found in the literature [51–53]. The $1/(4\pi R^2)$ in the evolution equations is for the two-parton density normalization, and R is viewed as the correlation length of two interacting partons. In a previous analysis of the proton [40], the two-parton correlation length R is fitted to be 3.98 GeV⁻¹. For different hadrons, the values of R are different and related to the radii of the hadrons. In this analysis of the pion and the kaon, R is a free parameter which should be determined with the global fit to the data.

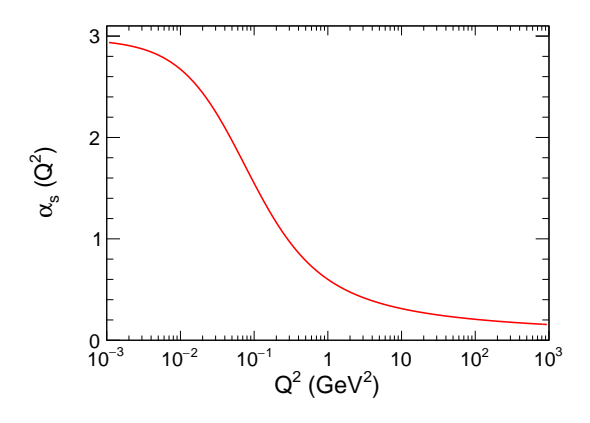


FIG. 1. The infrared-saturating strong coupling $\alpha_{\rm s}$ [41] used in this work.

The running strong coupling constant α_s is an important parameter in the QCD evolution equations. In this work, we use a renormalisation-group-invariant process-independent effective strong coupling constrained by the calculation of lattice QCD [41]. The effective strong coupling shows a saturated plateau approaching the infrared region, which agrees well with the experimental measurement of Bjorken sum rule at low Q^2 (< 1 GeV²). The saturated effective strong coupling is given by [41],

$$\alpha_{\rm s}(Q^2) = \frac{4\pi}{\beta_0 {\rm Ln}[(m_\alpha^2 + Q^2)/\Lambda_{\rm QCD}^2]},$$
 (8)

where $\beta_0 = (33-2n_{\rm f})/3$ refers to the one-loop β function coefficient, $n_{\rm f}$ is the number of flavors, $m_{\alpha} = 0.43$ GeV is the effective gluon mass owning to the dynamical breaking of scale invariance [41]. For the QCD cutoff, we chose $\Lambda_{\rm QCD} = 0.34~{\rm GeV}^2$. Fig. 1 shows the running strong coupling applied in this analysis, which has the saturated strong coupling around 3.

IV. DETERMINATIONS OF INPUT SCALE Q_0^2 AND PARTON-PARTON CORRELATION LENGTH R FOR PION AND KAON

As the nonperturbative input is taken as the MEM prediction, only the hadronic scale Q_0^2 and the parton-

parton recombination parameter R are left to be determined by the global analysis. We use the least square fit to find the optimal parameters for the pion and the kaon respectively. The reduced χ^2 for the fit is defined as,

$$\chi^2/\text{ndf} = \frac{1}{N_{\text{tot.}} - n_{\text{par.}}} \sum_{i}^{N_{\text{Exp.}}} \sum_{j}^{N_i} \frac{(D_j - T_j)^2}{\sigma_j^2},$$
 (9)

in which $N_{\rm tot.}$ is the total number of data points of all experiments, $n_{\rm par}=2$ is the number of free parameters in our analysis. $N_{\rm Exp.}$ is the number of experimental measurements used in the analysis; N_i is the number of data points for experiment i; D_j is one data point for the experimental observables; σ_j is the corresponding error of the data point D_j ; And T_j is the corresponding theoretical prediction of D_j . Specifically for this study, the experimental observables D_j are the valence quark distribution measured in DY process, and the structure function F_2 measured in the leading neutron tagged DIS process. In the least square fit, we use the MINUIT package to find the minimum χ^2 and the optimal parameters. In the analysis of pion PDFs, we take the DY data

by Fermilab E615 Collaboration [27] and the structure function data by H1 Collaboration at HERA [29]. For the analysis of kaon PDFs, we take the $u^{\rm K}/u^{\pi}$ data from CERN-NA3 experiment [24]. With the least square method, we get the hadronic scales of the nonperturbative inputs for the pion and the kaon, and the two-parton correlation length R, which are listed in table I. The qualities of the two fits are amazingly good. The parameter R for the parton-parton recombination strength is sensitive to the experimental data at small x (< 0.01), but not to the experimental data at large x. The CERN-NA3 data used to constrain kaon PDFs are at the large x > 0.2. Therefore it is impossible to determine the parameter R for the kaon, using the current NA3 data. The experimental data at small x for the kaon structure are highly needed, which can be accessed with the future electron-ion colliders [6, 54, 55]. In this analysis, we let the parameter R to be the same for both the pion and the kaon, for they are in the same meson octet and both of the Glodstone boson nature.

In this work, the hadronic scale for the pion is $Q_0^2 = 0.129 \text{ GeV}^2$, and the hadronic scale for the kaon is $Q_0^2 = 0.110 \text{ GeV}^2$. In the previous and similar analysis of the proton using the pure valence quark input, the hadronic scale is $Q_0^2 = 0.067 \text{ GeV}^2$. The smaller the hadron size is, the higher resolution scale is needed to just resolve the minimum quark components of the hadron. Since the sizes of pion and kaon are smaller than that of proton, the input hadronic scales should be higher than that of proton. The obtained hadronic scales for the pion and the kaon are within the naive expectations. The parton-parton correlation length for the pion and the kaon is obtained to be $R = 2.392 \text{ GeV}^{-1}$ in this work, which is smaller than that of the proton (3.98 GeV^{-1}) determined in a previous work. This also can be understood as resulting from the smaller radius of the

TABLE I. The obtained input scale Q_0^2 and the parton-parton correlation length R for the pion and the kaon, from the fittings to the popular experimental data up to date.

	Q_0^2/GeV^2	R/GeV^{-1}	χ^2/ndf	Experiment	N points
π	0.129	2.392	0.864	E615 + H1	40 + 29
K	0.110	2.392	0.750	CERN-NA3	8

meson, since the correlation length R is proportional to the radius of the hadron. The obtained input hadronic scales Q_0^2 and parton-parton recombination parameter R for the pion and the kaon are within the theoretical esitmations.

V. RESULTS AND DISCUSSIONS

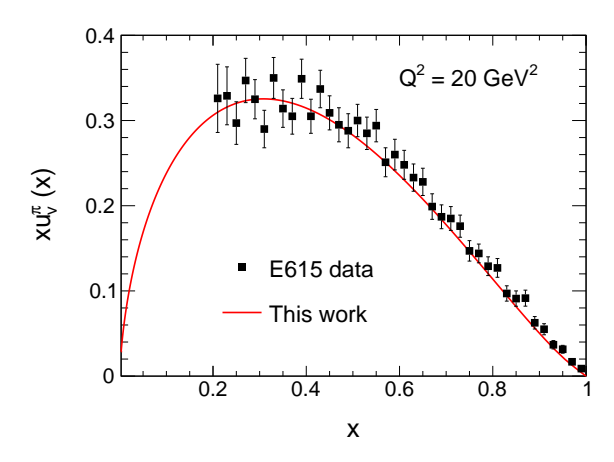


FIG. 2. Comparisons of our predicted up valence quark distribution of the pion with E615 experimental data [27].

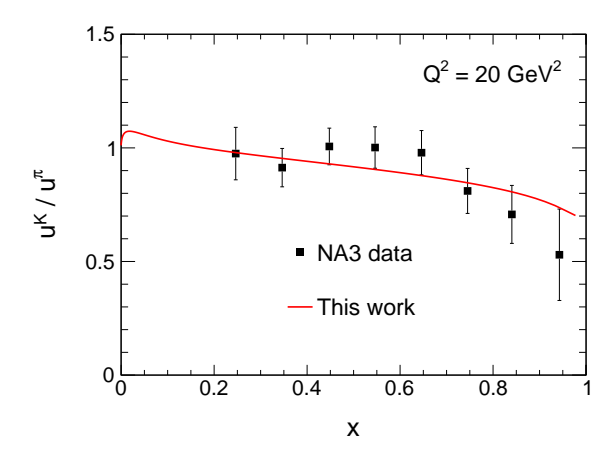


FIG. 3. Comparisons of our predicted ratio $u^{\rm K}/u^{\pi}$ as a function of x with CERN-NA3 experimental data [24].

With the obtained hadronic scales, we calculate pion

and kaon parton distribution functions with QCD evolution equations. Fig. 2 shows our obtained pionic valence quark distribution compared with the Drell-Yan data from Fermilab E615 experiment [27]. Fig. 3 shows our obtained ratio between kaon up quark distribution and pion up quark distribution, compared with the CERN-NA3 Drell-Yan data from the pion and the kaon beams [24]. We find that both pion and kaon PDFs determined in this work are consistent with the experimental measurements in the large x region (x > 0.2). Our prediction of u^{K}/u^{π} goes down smaller than one as x goes from 0.2 to 1. The CERN-NA3 experiment shows that the ratio $u^{\rm K}/u^{\pi}$ is smaller than one when x>0.7. We need more precise experimental data to figure out where the kaon up quark distribution starts to be smaller than the pion up quark distribution.

By measuring the leading neutron tagged deep inelastic scattering of e-p and using the one-pion exchange model, ZEUS and H1 Collaborations at HERA extracted the pionic structure function at small x [28, 29]. Fig. 4 shows the comparisons among the obtained pion structure function at small x, the H1 experimental data [29], and the GRS model predictions [30]. In the sea quark region, our global analysis with the MEM nonperturbative input agrees well with the experimental observations. The previous GRS analysis is also close to the H1 data, which is a pioneering work using the dynamical parton model [30]. Fig. 5 shows the comparisons among the obtained pion structure function at small x, the ZEUS experimental data [28], and the GRS model predictions [30]. In the analysis by ZEUS Collaboration, the pion flux in LN-DIS is evaluated by the effective field (EF) formula or the addictive quark model (AQM) formula [28]. Both our results and the GRS results are between the two experimental data sets from two different analysis methods. The pion structure function from this analysis is closer to the ZEUS data applying the EF method. Note that the ZEUS data are not included in our global fit. It is very interesting to find that our prediction is similar to the GRS model prediction in the region of $x < 10^{-3}$, while there is big discrepancy between our prediction and the GRS model prediction around x = 0.1. The future experimental measurements on electron-ion colliders will help clarify the difference among different models.

Fig. 6 shows the obtained valence quark, sea quark and gluon distributions of the pion at high Q^2 based on this global analysis. Fig. 7 shows the obtained valence quark, sea quark and gluon distributions of the kaon at high Q^2 based on this global analysis. In this analysis, the nonperturbative input and the parton-parton correlation length R are the same for the pion and the kaon. The PDFs of the pion and the kaon exhibit a very small difference since there is only a little bit difference between the input hadronic scales for the pion and the kaon.

Fig. 8 demonstrates the obtained kaon PDFs in the large x region. We find that the valence up quark distribution and the valence anti-strange quark distribution are obviously different in the kaon. This is due to the

mass-dependent splitting kernels for the QCD evolution. Similar to a recent work [11], we apply a modified QCD splitting kernel function for the strange quark distribution evolution starting from a very low Q_0^2 , since the strange quark is significantly heavier than the up and down quark. The strange quark has a smaller probability of radiating the gluons, hence the valence strange quark distribution is higher than the valence up quark distribution. Fig. 9 shows the ratio of the strange valence quark distribution to the up valence quark distribution as a function of Q^2 . The mass effect of the strange quark splitting near the hadronic scale is obvious but not large. In the large x region, the strange quark distribution is just around 15% higher.

The large-x behavior of the valence quark distribution is an interesting topic in theory, which can be calculated with the quark number counting rule [56, 57] or the perturbative QCD predictions [35–37]. The large-x behavior is usually described by,

$$xf_{\mathbf{i}}(x,Q^2) \stackrel{x \to 1}{\longrightarrow} (1-x)^{\beta_{\mathbf{i}}},$$
 (10)

with the parton distribution going down as the power β of (1-x). With the determined PDFs of the pion and the kaon at high Q^2 , we performed the fits to them and extracted the corresponding powers β , which are listed in table II. The coefficients β are around 1 for the valence quark distributions; The coefficients β are around 2 for the sea quark distributions of u and d: The coefficient β is around 3.5 for the strange sea quark distribution; And the coefficients β are around 3 for the gluon distributions. In the fits, we use the function form $Cx^{\alpha}(1-x)^{\beta}$, and the fit range is 0.2 < x < 1. At large x, the Brodsky-Farrar quark counting rule predicts that $xf_i \sim (1-x)^{2n_s-1}$, where $n_{\rm s}$ is the minimum number of spectator partons [56, 57]. These are defined to be the partons that are not struck in the hard-scattering process, since it is assumed that, in the limit $x \to 1$, there can be no momentum left for any of the partons other than the struck parton. In a meson made of one quark and one anti-quark, one has for a valence quark, $n_{\rm s}=1$ and thus $\beta_{\rm v}=1$; for a gluon, $n_{\rm s}=2$ and $\beta_{\rm g}=3$; for a sea quark, $n_{\rm s}=3$ and $\beta_{\rm s}=5$. Thus our results are consistent with the counting rule for the valence quark distribution and the gluon distribution. From perturbative QCD, the β for the valence quark distribution is 2 in the asymptotic region [35–37]. Our extracted value in the LO analysis is smaller than 2. The discrepancy should be understood with the NLO corrections or the resummation of soft gluons [38]. In short, the large-x behavior of the obtained valence quark distribution is between the quark number counting rule and the perturbative QCD preditions.

In the small x region, the x-dependences of the quark and gluon distributions are described well by Regge theory [57, 58]. The small-x behavior is usually described by,

$$xf_{i}(x,Q^{2}) \stackrel{x\to 0}{\longrightarrow} x^{\alpha_{i}}.$$
 (11)

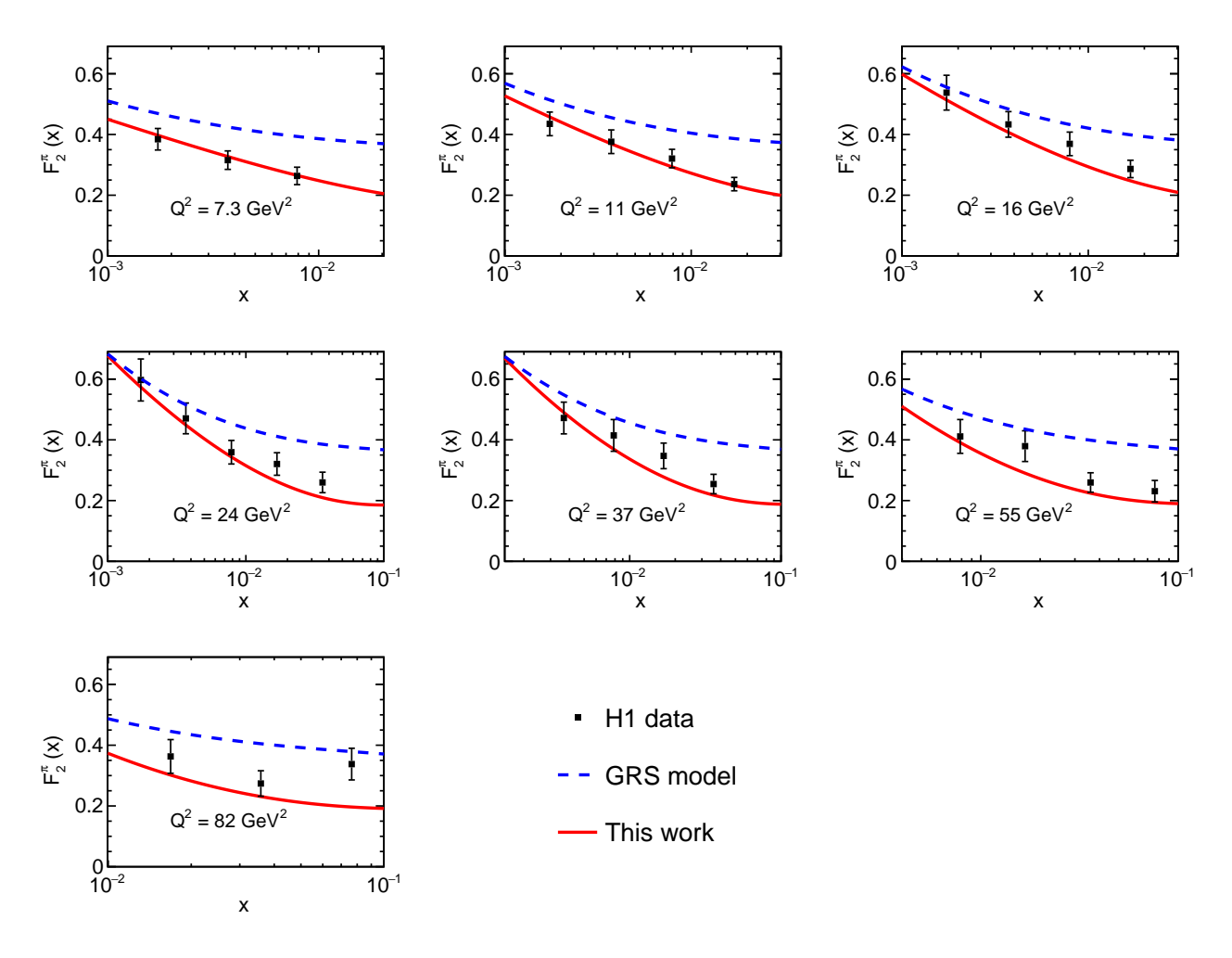


FIG. 4. Our predicted structure function $F_2^{\pi}(x,Q^2)$ compared with H1 data [29], and GRS model predictions [30].

TABLE II. Assuming PDFs obey $\propto (1-x)^{\beta}$ in the large x region approaching 1, we list the obtained values of the power β for valence quark, sea quark and gluon distributions of the pion and the kaon at $Q^2=20~{\rm GeV}^2$. The β values are extracted from the fits in the range of 0.6 < x < 1.

	$\beta_{ m u_v}$	$\beta_{\bar{\mathbf{s}}_{\mathbf{v}}}$	$eta_{ar{u}_{ ext{sea}}}$	$\beta_{ar{s}_{sea}}$	$\beta_{ m g}$
π	1.28	-	2.18	2.18	2.68
K	1.38	1.54	2.41	3.49	2.82

With the determined PDFs of the pion and the kaon at high Q^2 , we performed the fits to them and extracted the corresponding powers α , which are listed in table III. The coefficients α are around 0.5 for the valence quark distributions; The coefficients α are around -0.2 for the sea quark distributions; The coefficient α is around 1 for the strange valence quark distribution; And the coefficients α are around -0.25 for the gluon distributions. In the fits, we use the function form Cx^{α} , and the fit range is $10^{-6} < x < 0.1$. The Regge theory [57, 58] predicts $\alpha = 0.5$ for valence quark distributions, $\alpha = -0.08$ for

TABLE III. Assuming PDFs obey $\propto x^{\alpha}$ in the small x region approaching 0, we list the obtained values of the power α for valence quark, sea quark and gluon distributions of the pion and the kaon at $Q^2=20~{\rm GeV}^2$. The α values are extracted from the fits in the range of $10^{-6} < x < 10^{-1}$.

	$\alpha_{ m u_v}$	$lpha_{ar{ ext{s}}_{ ext{v}}}$	$lpha_{ar{ ext{u}}_{ ext{sea}}}$	$lpha_{ar{ ext{s}}_{ ext{sea}}}$	$\alpha_{ m g}$
π	0.59	-	-0.19	-0.19	-0.25
K	0.57	1.19	-0.2	-0.21	-0.25

sea quark and gluon distributions. With the resummation of double logarithms, the Regge theory then gives $\alpha=0.63$ for valence quark distributions, and $\alpha=-0.2$ for sea quark and gluon distributions. The PDFs of the pion and the kaon determined in this analysis are consistent with the predictions of Regge theory [57, 58].

The moments of the momentum distributions of quarks are usually calculated in theory. To compare with the theoretical calculations, we also provide the moments of the obtained parton distributions of the pion and the kaon. The moment of the parton momentum fraction

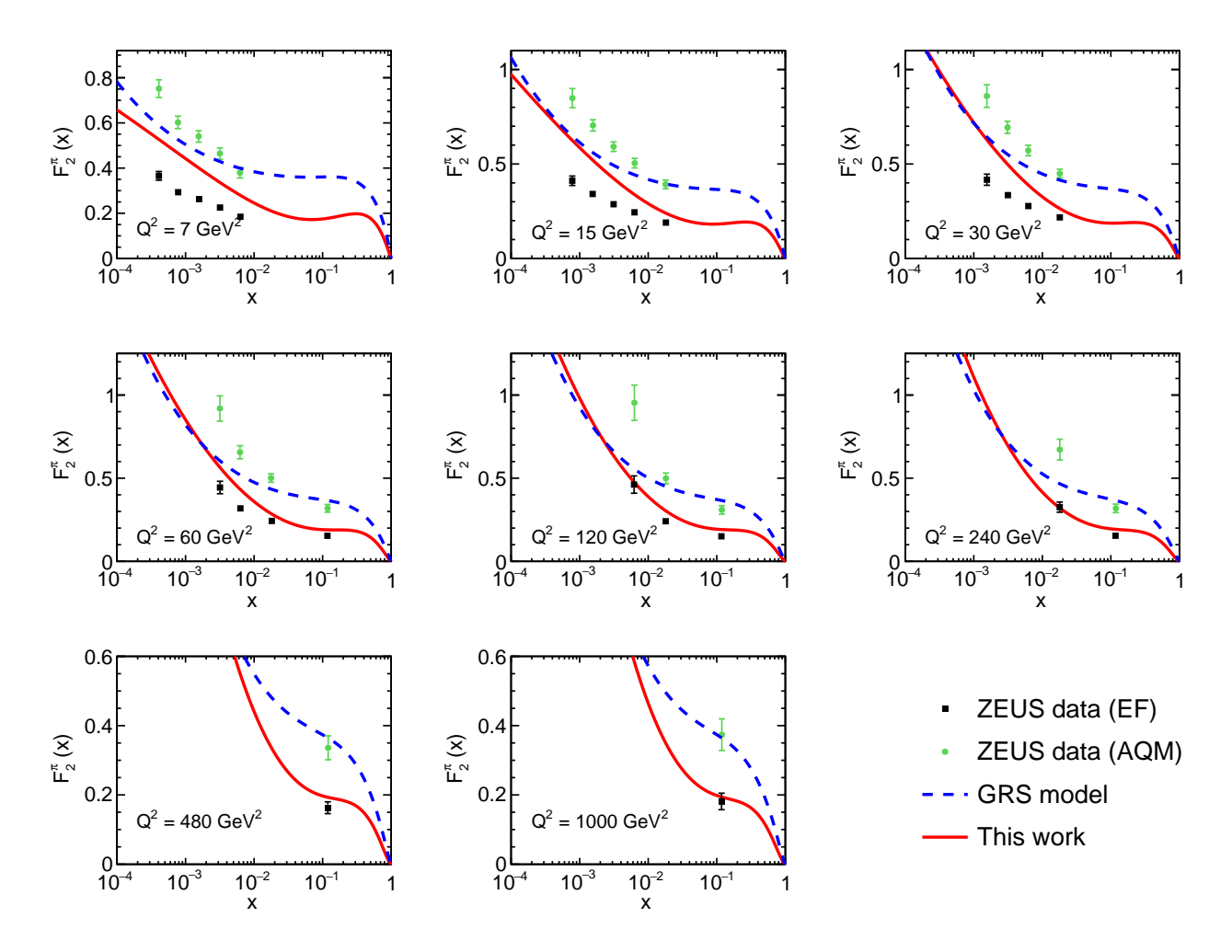


FIG. 5. Our predicted structure function $F_2^{\pi}(x,Q^2)$ compared with the experimental data by ZEUS Collaboration [28], and the GRS model predictions [30]. The pion structure function data are extracted using two different formulae (EF model and AQM model) [28].

distribution used in this work is defined as,

$$\langle x^n \rangle_f = \int_0^1 x^n f(x, Q^2) dx. \tag{12}$$

The first three moments of the quark distributions of the pion are listed in table IV. The first three moments of the quark distributions of the kaon are listed in table V. Lattice QCD and Dyson-Schwinger equations are two main nonperturbative QCD approaches in understanding the strong interaction. From the tables, we can see that the moments of the pion and the kaon determined in this analysis are consist with QCD theory. The DSE is taken from the recent work by Z. F. Cui et al. [11, 17], and the LQCD result is taken from Refs. [12, 59, 60].

Fig. 10 shows the gluon momentum distributions of the pion, the kaon and the proton at a high Q^2 . We find that the gluon distributions of the pion and the kaon are quite similar, which are lower than the gluon distribution of the proton at small x. Fig. 11 shows the sea quark momentum distributions of the pion, the kaon and the

TABLE IV. Comparisons of our predicted moments $\langle x \rangle$, $\langle x^2 \rangle$, $\langle x^3 \rangle$ of quark distributions of the pion with some other theoretical calculations, at $Q^2 = 4 \text{ GeV}^2$.

	$\langle x \rangle^{\pi}$	$\langle x^2 \rangle^{\pi}$	$\langle x^3 \rangle^{\pi}$
DSE [17] $(u_{\rm v})$	0.24	0.098	0.049
LQCD [59] (u_v)	0.273	0.107	0.048
LQCD [12] (u_v)	0.24	0.09	0.043
LFHQCD [19] (u_v)	0.233	0.102	0.056
NJL model [61] $(u_{\rm v})$	0.236	0.103	0.057
This work (u_{v})	0.241	0.107	0.060

proton at a high Q^2 . We find that the sea quark distributions of the pion and the kaon are quite similar, which are lower than the sea quark distribution of the proton at small x as well. The other finding is that the strange sea quark distribution is higher than the up sea quark distribution in the kaon. This is due to the modified splitting kernels used for the kaon in the DGLAP evolution.

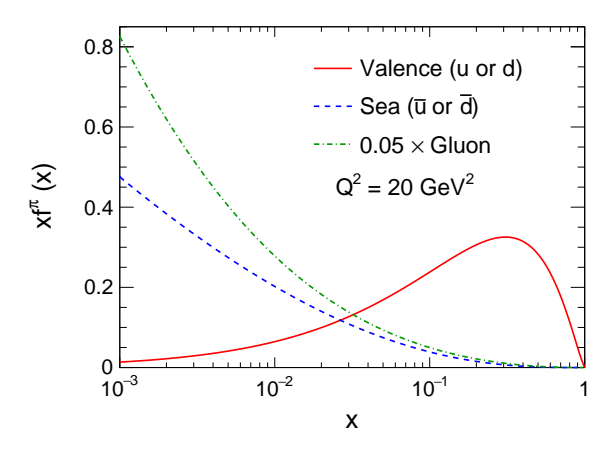


FIG. 6. The valence quark, sea quark and gluon distributions of the pion from this work.

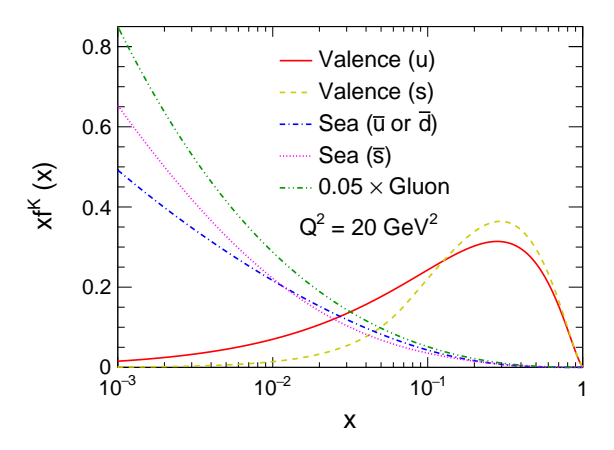


FIG. 7. The valence quark, sea quark and gluon distributions of the kaon from this work.

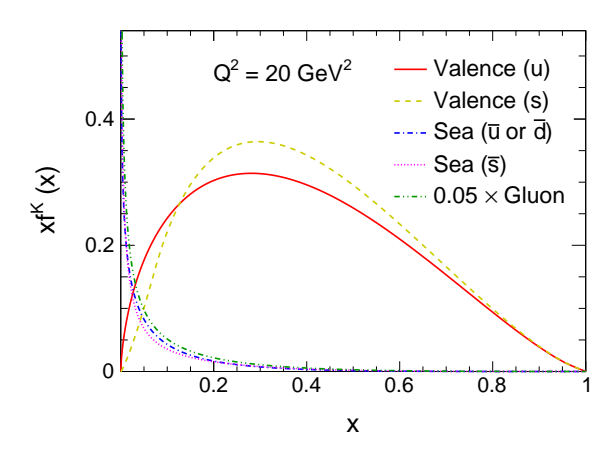


FIG. 8. The valence quark, sea quark and gluon distributions of the kaon from this work, in the range of large x.

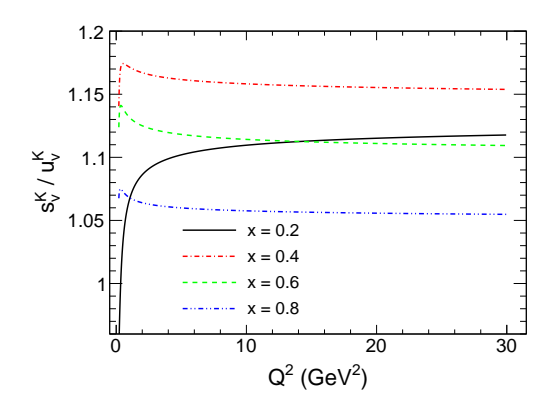


FIG. 9. The obtained ratio $s_{\rm v}^{\rm K}/u_{\rm v}^{\rm K}$ as a function of Q^2 with the strange quark mass effect is considered in the parton splitting processes of the DGLAP evolution.

TABLE V. Comparisons of our predicted moments $\langle x \rangle$, $\langle x^2 \rangle$, $\langle x^3 \rangle$ of quark distributions of the kaon with some other theoretical calculations, at $Q^2 = 27 \text{ GeV}^2$.

	$\langle x \rangle^{\mathrm{K}}$	$\langle x^2 \rangle^{\mathrm{K}}$	$\langle x^3 \rangle^{\mathrm{K}}$
DSE [11] (u_{v})	0.19	0.067	0.030
DSE [11] (\bar{s}_{v})	0.23	0.085	0.040
LQCD [60] (u_v)	0.193	0.080	0.042
LQCD [60] (\bar{s}_{v})	0.267	0.123	0.070
This work $(u_{\rm v})$	0.192	0.0747	0.0382
This work (\bar{s}_{v})	0.207	0.0828	0.0422

VI. SUMMARY

In this analysis, we have obtained the hadronic scales for the pion and the kaon, where there are only the valence components of the hadrons. The input hadronic scales for the pion and the kaon are around $0.1~{\rm GeV^2}$, which are slightly higher than that of the proton [40]. In our analysis, the input parton distributions of merely valence quarks are the suggested uniform distribution by

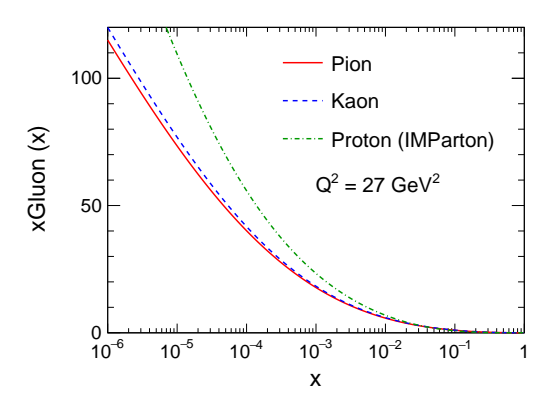


FIG. 10. The comparisons of the gluon distributions inside the pion, the kaon, and the proton at $Q^2=27~{\rm GeV}^2$.

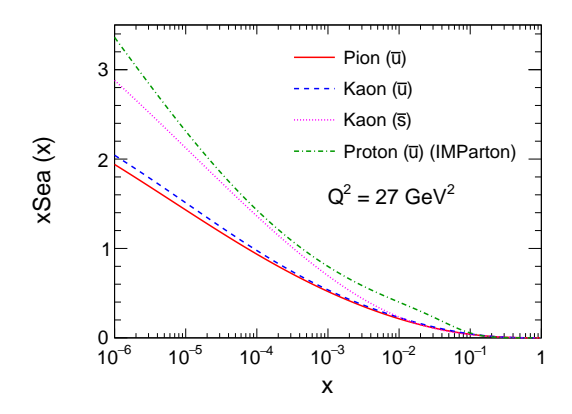


FIG. 11. The comparisons of the sea quark distributions inside the pion, the kaon, and the proton at $Q^2 = 27 \text{ GeV}^2$.

a maximum entropy estimation. The χ^2/ndf for both fits to the pion data and to the kaon data are less than 1. The determined parton distributions of the pion and the kaon are shown to be consistent with the DY data by E615 and the leading neutron tagged DIS data by H1 and ZEUS at HERA. Via this analysis, we can see that the nonperturbative input from maximum entropy method is reasonable. For the practical applications based on this analysis, we provide a software package for the users to access the obtained PDFs of the pion and the kaon, which can be found on the web [62].

In this work, we use the $\overline{\mathrm{DGLAP}}$ equations with the parton-parton recombination corrections. By the global fit to the current experimental data, we get the parton-parton correlation length R of the nonlinear evolution for the pion and the kaon, which is smaller than that of the proton. This is within the naive expectation that the parton-parton correlation length is proportional to the size of the hadron. Since the radii of the pion and the kaon are smaller than that of the proton, it is natural to have the two-parton fusion probability higher inside the pion and the kaon. The QCD evolution with the parton-parton recombination corrections is an approximate but simple bridge to connect the pure valence nonperturbative input with the experimental measurements at the hard scales.

The purely dynamical parton model is used in this work. In this dynamical parton model, there are no sea quarks and gluons at the input hadronic scale. Therefore, the sea quark and gluon distributions at high scales are totally generated from the standard QCD evolution. In this way, the sea quark and gluon distributions are better constrained, and they are suggested to be very useful in a lot of future applications.

The large-x and small-x behaviors of the obtained parton distribution functions of the pion and the kaon are studied. We find that the power law at large x are between the quark number counting rule and the perturbative QCD predictions. And the power law behavior at small x are well consistent with the Regge theory calculations with the double logarithmic resummation considered. We also calculate the first three leading moments $\langle x \rangle, \langle x^2 \rangle, \langle x^3 \rangle$, and compare them with the LQCD calculations and other model calculations. The consistencies are found. The global analysis based on the purely dynamical parton model provides a clear picture on how do the parton distributions come from.

We have acquired the PDFs of the pion and the kaon, which are suggested to be used in a lot of phenomenological applications. We also see that there are some rooms left to be improved in the future, such as using the DGLAP equations at next-to-leading order with the parton-parton recombination corrections. Most importantly, much more experimental data of the pion and the kaon are needed to constrain the sea quark and gluon distributions of the mesons. Especially, the kaon structure experiment is highly needed, as there are few data on the kaon structure for now. In the future, the updating and the new facilities will provide much more data in settling down the questions, such as the COMPASS++/AMBER with the pion and kaon beams [63], JLab [64], EicC [6, 54] and EIC [55] with the tagged DIS techniques.

ACKNOWLEDGMENTS

This work is supported by the Strategic Priority Research Program of Chinese Academy of Sciences under the Grant NO. XDB34030301.

Y. Nambu, Phys. Rev. 117, 648 (1960).

^[2] J. Goldstone, A. Salam, and S. Weinberg, Phys. Rev. 127, 965 (1962).

^[3] P. Maris, C. D. Roberts, and P. C. Tandy, Phys. Lett. B 420, 267 (1998), arXiv:nucl-th/9707003.

^[4] C. D. Roberts, in 27th International Nuclear Physics Conference (2019) arXiv:1909.12832 [nucl-th].

^[5] C. D. Roberts and S. M. Schmidt (2020) arXiv:2006.08782 [hep-ph].

^[6] X. Chen, F.-K. Guo, C. D. Roberts, and R. Wang (2020) arXiv:2008.00102 [hep-ph].

^[7] X.-D. Ji, Phys. Rev. Lett. 74, 1071 (1995), arXiv:hep-ph/9410274

^[8] Y.-B. Yang, J. Liang, Y.-J. Bi, Y. Chen, T. Draper, K.-F. Liu, and Z. Liu, Phys. Rev. Lett. 121, 212001 (2018), arXiv:1808.08677 [hep-lat].

^[9] C. Lorcé, Eur. Phys. J. C 78, 120 (2018) arXiv:1706.05853 [hep-ph].

^[10] Y. Chen, (2020), arXiv:2010.00900 [hep-ph].

^[11] Z.-F. Cui, M. Ding, F. Gao, K. Raya, D. Binosi, L. Chang, C. D. Roberts, J. Rodríguez-Quintero, and S. M. Schmidt, (2020), arXiv:2006.14075 [hep-ph].

- [12] W. Detmold, W. Melnitchouk, and A. W. Thomas, Phys. Rev. D 68, 034025 (2003), arXiv:hep-lat/0303015.
- [13] C. Shugert, X. Gao, T. Izubichi, L. Jin, C. Kallidonis, N. Karthik, S. Mukherjee, P. Petreczky, S. Syritsyn, and Y. Zhao, in 37th International Symposium on Lattice Field Theory (2020) arXiv:2001.11650 [hep-lat].
- [14] R. S. Sufian, C. Egerer, J. Karpie, R. G. Edwards, B. Joó, Y.-Q. Ma, K. Orginos, J.-W. Qiu, and D. G. Richards, Phys. Rev. D 102, 054508 (2020), arXiv:2001.04960 [heplat].
- [15] X. Gao, L. Jin, C. Kallidonis, N. Karthik, S. Mukherjee, P. Petreczky, C. Shugert, S. Syritsyn, and Y. Zhao, (2020), arXiv:2007.06590 [hep-lat].
- [16] T. Nguyen, A. Bashir, C. D. Roberts, and P. C. Tandy, Phys. Rev. C 83, 062201 (2011), arXiv:1102.2448 [nucl-th].
- [17] C. Chen, L. Chang, C. D. Roberts, S. Wan, and H.-S. Zong, Phys. Rev. D 93, 074021 (2016), arXiv:1602.01502 [nucl-th].
- [18] M. Ding, K. Raya, D. Binosi, L. Chang, C. D. Roberts, and S. M. Schmidt, Phys. Rev. D 101, 054014 (2020), arXiv:1905.05208 [nucl-th].
- [19] G. F. de Teramond, T. Liu, R. S. Sufian, H. G. Dosch, S. J. Brodsky, and A. Deur (HLFHS), Phys. Rev. Lett. 120, 182001 (2018), arXiv:1801.09154 [hep-ph].
- [20] J. Lan, C. Mondal, S. Jia, X. Zhao, and J. P. Vary, Phys. Rev. Lett. 122, 172001 (2019), arXiv:1901.11430 [nucl-th].
- [21] A. Szczepaniak, C.-R. Ji, and S. R. Cotanch, Phys. Rev. D 49, 3466 (1994), arXiv:hep-ph/9309284.
- [22] T. Frederico and G. Miller, Phys. Rev. D 50, 210 (1994).
- [23] A. Watanabe, C. W. Kao, and K. Suzuki, Phys. Rev. D 94, 114008 (2016), arXiv:1610.08817 [hep-ph].
- [24] J. Badier et al. (Saclay-CERN-College de France-Ecole Poly-Orsay), Phys. Lett. B 93, 354 (1980).
- [25] J. Badier et al. (NA3), Z. Phys. C 18, 281 (1983).
- [26] B. Betev et al. (NA10), Z. Phys. C 28, 9 (1985).
- [27] J. Conway et al., Phys. Rev. D 39, 92 (1989).
- [28] S. Chekanov et al. (ZEUS), Nucl. Phys. B 637, 3 (2002), arXiv:hep-ex/0205076.
- [29] F. Aaron et al. (H1), Eur. Phys. J. C 68, 381 (2010), arXiv:1001.0532 [hep-ex].
- [30] M. Gluck, E. Reya, and I. Schienbein, Eur. Phys. J. C 10, 313 (1999), arXiv:hep-ph/9903288.
- [31] P. Sutton, A. D. Martin, R. Roberts, and W. Stirling, Phys. Rev. D 45, 2349 (1992).
- [32] P. Barry, N. Sato, W. Melnitchouk, and C.-R. Ji, Phys. Rev. Lett. 121, 152001 (2018), arXiv:1804.01965 [hep-ph].
- [33] R. Towell et al. (NuSea), Phys. Rev. D 64, 052002 (2001), arXiv:hep-ex/0103030.
- [34] I. Novikov et al., Phys. Rev. D 102, 014040 (2020), arXiv:2002.02902 [hep-ph].
- [35] Z. Ezawa, Nuovo Cim. A 23, 271 (1974).
- [36] G. R. Farrar and D. R. Jackson, Phys. Rev. Lett. 35, 1416 (1975).
- [37] E. L. Berger and S. J. Brodsky, Phys. Rev. Lett. 42, 940 (1979).

- [38] M. Aicher, A. Schafer, and W. Vogelsang, Phys. Rev. Lett. 105, 252003 (2010), arXiv:1009.2481 [hep-ph].
- [39] M. Gluck and E. Reya, Nucl. Phys. B 130, 76 (1977).
- [40] R. Wang and X. Chen, Chin. Phys. C 41, 053103 (2017), arXiv:1609.01831 [hep-ph].
- [41] Z.-F. Cui, J.-L. Zhang, D. Binosi, F. de Soto, C. Mezrag, J. Papavassiliou, C. D. Roberts, J. Rodríguez-Quintero, J. Segovia, and S. Zafeiropoulos, Chin. Phys. C 44, 083102 (2020), arXiv:1912.08232 [hep-ph].
- [42] L. Gribov, E. Levin, and M. Ryskin, Phys. Rept. 100, 1 (1983).
- [43] A. H. Mueller and J.-w. Qiu, Nucl. Phys. B 268, 427 (1986).
- [44] X. Chen, J. Ruan, R. Wang, P. Zhang, and W. Zhu, Int. J. Mod. Phys. E 23, 1450057 (2014), arXiv:1306.1872 [hep-ph].
- [45] L. Chang, C. Mezrag, H. Moutarde, C. D. Roberts, J. Rodríguez-Quintero, and P. C. Tandy, Phys. Lett. B 737, 23 (2014), arXiv:1406.5450 [nucl-th].
- [46] C. Han, H. Xing, X. Wang, Q. Fu, R. Wang, and X. Chen, Phys. Lett. B 800, 135066 (2020), arXiv:1809.01549 [hep-ph].
- [47] R. Wang and X. Chen, Phys. Rev. D 91, 054026 (2015), arXiv:1410.3598 [hep-ph].
- [48] Y. L. Dokshitzer, Sov. Phys. JETP 46, 641 (1977).
- [49] V. Gribov and L. Lipatov, Sov. J. Nucl. Phys. 15, 438 (1972).
- [50] G. Altarelli and G. Parisi, Nucl. Phys. B **126**, 298 (1977).
- [51] W. Zhu, Nucl. Phys. B 551, 245 (1999), arXiv:hep-ph/9809391.
- [52] W. Zhu and J.-h. Ruan, Nucl. Phys. B 559, 378 (1999), arXiv:hep-ph/9907330.
- [53] W. Zhu and Z.-q. Shen, HEP. & NP. Vol. 2, ,109 (2005), arXiv:hep-ph/0406213.
- [54] X. Chen, PoS DIS2018, 170 (2018), arXiv:1809.00448 [nucl-ex].
- [55] A. Accardi et al., Eur. Phys. J. A 52, 268 (2016), arXiv:1212.1701 [nucl-ex].
- [56] S. J. Brodsky and G. R. Farrar, Phys. Rev. Lett. 31, 1153 (1973).
- [57] R. D. Ball, E. R. Nocera, and J. Rojo, Eur. Phys. J. C 76, 383 (2016), arXiv:1604.00024 [hep-ph].
- [58] T. Regge, Nuovo Cim. 14, 951 (1959).
- [59] C. Best, M. Gockeler, R. Horsley, E.-M. Ilgenfritz, H. Perlt, P. E. Rakow, A. Schafer, G. Schierholz, A. Schiller, and S. Schramm, Phys. Rev. D 56, 2743 (1997), arXiv:hep-lat/9703014.
- [60] H.-W. Lin, J.-W. Chen, Z. Fan, J.-H. Zhang, and R. Zhang, (2020), arXiv:2003.14128 [hep-lat].
- [61] R. Davidson and E. Ruiz Arriola, Phys. Lett. B 348, 163 (1995).
- [62] "lukeronger/piIMParton," https://github.com/lukeronger/piIMParton, accessed: 2020-10-26.
- [63] B. Adams et al., (2018), arXiv:1808.00848 [hep-ex].
- [64] "Measurement of Tagged Deep Inelastic Scattering (TDIS)," https://www.jlab.org/exp_prog/proposals/15/PR12-15-006.pdf, accessed: 2020-10-26.